Adaptive Neuro-Fuzzy Control for Minimizing Submodule Capacitance in Modular Multilevel Converters for Wind Energy Systems

K. Siva Agora Sakthivel Murugan^{1*}, Mashhoor Al Tarayrah², Mounir Bouzguenda³, Anas A. Amro²

Department of EEE, Tamilnadu College of Engineering, Coimbatore Tamilnadu, India
 Department of Technology, College of Professions and Applied Sciences,
 Hebron University, Hebron, Palestine, mtarayrah8@gmail.com anasamro@hebron.edu
 Department of Electrical Engineering, College of Engineering, King Faisal University

Al Ahsa, 31982, Saudi Arabia, mbuzganda@kfu.edu.sa

* Correspondence: Sasvm2k6@gmail.com

Abstract: The direct-drive permanent magnet synchronous generator (PMSG) and modular multilevel converter (MMC)-based offshore DC wind turbine has emerged as a strong contender for the large-capacity wind energy conversion system (WECS). Few technical challenges exist for MMC when used in medium potential WECS for PMSG. The important one is the enormous submodule (SM) voltage fluctuation brought on by the PMSG phase current, which has a high amplitude and low frequency. But because this topology's capacitor voltage is floating, a larger capacitor is needed, which raises the project's cost. This research suggests a minimum voltage ripple control across the capacitor for an MMC-based wind energy conversion systems. For wind energy conversion systems based on MMC, a different control method known as CCVR (Constant Capacitance Voltage Ripple) is suggested. The voltage ripple on the CM capacitor can be greatly reduced by using this method since it allows for the inclusion of the propagating current's second harmonic component. Because of this, smaller SM capacitors can be used. This paper introduces a constant capacitance voltage ripple (CCVR) control strategy and an ANFIS-based controller to address these challenges, aiming to reduce SM capacitor size while maintaining optimal system performance.

Keywords: PMSG, MMC, WECS, submodule, CCVR, ANFIS

1. Introduction

Full DC wind power parks using DC parallel connection and high-voltage DC transmission have drawn a lot of attention recently as a result of the growth in power generating capacity of wind power parks and the expansion of offshore distance. attention. Both types of lines can be connected to and converted by the high voltage alternating current HVDC converter. There are currently two distinct converter topologies. The interoperability challenges of new modular voltage source converter (VSC) topologies HVDC systems should be addressed concurrently with the rapid growth of power systems brought on by the demand for more interconnected networks. The diversity of modern distributed energy supplies and the rising need for worldwide energy consumption are what are forcing dc power systems to give more

sophisticated capabilities than ever before. From systems based online-commutated converters (LCC), via VSC, to systems based on MMC, HVDC technology has improved recently [1]-[3].

The MMC still requires sizable, large DC storage capacitors to balance off the massive power pulsations caused by the single-phase AC to DC conversion process in its arms. Due to its distinct notable features that make it perfect for VSC-based HVDC, the modular multilevel converter, one of the existing classes of high-power converter topologies, has attracted a lot of study interest recently [4]. Due to its benefits including modularity, high efficiency, and flexible expandability, the MMC, which was first presented in 2003, has emerged as the topology with the greatest potential for next-generation medium/high-voltage applications. The MMC has gained popularity in recent years for medium-voltage drive applications [5].

Voltage changes are inversely related to the MMC's operating frequency. Hoist, conveyor, and mill applications—all zero/low speed, high torque scenarios—cannot withstand significant voltage changes. Overmodulation and decreased system dependability may result from this. The most popular technique for reducing the voltage fluctuation of low-speed MMC capacitors is the current injection-based approach [6]. Low-frequency capacitor voltage variations can be minimized [7], but the device is subjected to more current stress. For MMC, a better implantation method is suggested to lessen the strains already present in the device. Still needed is high amplitude current injection.

This is due to the fact that subunit IGBTs are frequently produced with maximum voltage ratings that are twice as high as the subunit capacitor's DC voltage rating. Two further methods for reducing voltage ripple on the MMC submodule capacitors during low-speed operation [9] - [12]. However, because the loop current component has high peak values and is given to make up for the subunit capacitor's huge ripple voltage during machine startup, there is severe overcurrent in the MMC arms.

Current injection-based solutions call for the injection of high-amplitude circulating currents because device current stress is quite high, particularly at low speeds and high torque circumstances. Alternative methods to lessen voltage variations on MMC capacitors at low speeds include using variable DC voltage approaches [13] through [15]. Large amounts of SM capacitance are required for medium voltage low speed drives, which is more than the variable DC voltage approach can handle in terms of regulating MMC capacitor voltage swings. The following are some of the main benefits of MMCs over conventional two-voltage source converters.

(i) Because of the low bridge arm voltage and current change rates of semiconductor devices like IGBT, switching transients are not easily influenced by them, assuring their stable and secure operation.

- (ii) In high-voltage, large-capacity MMC, there are a lot of SMs, a good voltage step waveform, high-quality components, and very little harmonic content, so no filter is necessary.
- (iii) The modular structure can readily be expanded and altered to accommodate changing engineering requirements as well as the demands of more sophisticated power systems [16]-[18].

The MMC's capacitors are not, however, coupled to the DC bus in the same way as traditional 2-level and 3-level converters. The submodule (SM) contains its capacitor. The SM capacitors will experience arm current flow when the MMC is in operation. The capacitor voltage will fluctuate as a result of this, the MMC often needs a capacitor with a high capacitance [19]-[20]. The converter's size as well as price may increase due to the huge capacitor.

For the MMC-based medium voltage wind converters, we suggest CCVR (constant capacitance voltage ripple) regulation in this study. To balance the fundamental voltage component, the capacitor's second harmonic voltage component is changed.

The modelling equations of the MMC based WECS are also presented in this section. Section 4 analyses the proposed ANFIS controller details in brief.

2. Description of the MMC structure Methods

The MMC topology's primary building blocks are depicted in Figure 1. Arms of the converter are formed by stacked converter cells called sub-modules. To get the appropriate number of levels and rated voltage, SMs can be stacked on top of one another. The converter leg is constructed from two stacked arms. To get the appropriate number of stages, more legs can be piled. The most crucial component of the MMC is the topology of the SM, which establishes the fundamental characteristics of the converter.

SM is the fundamental part and component needed to implement the modularization of the MMC topology. When several SMs are connected in series, an MMC arm that serves as a regulated voltage source is produced. The voltage (varm) is dependent on the number of SMs connected or bypassed within the arm as well as the number of voltage levels on each SM output. In addition to the MMC's high-level functionality, the topology of each individual SM further specifies a number of converter properties, including the converter's capacity for error isolation, its level of dependability and redundancy, and its need for internal voltage balancing. The primary internal properties of the MMC, including capacitor voltage, switching frequency, conductance, and switching loss, are similarly impacted by the SM structure.

- 3. Proposed control methodology
- 3.1 MMC Based WECS

Figure 2 depicts the usual layout of an MMC-based WECS.

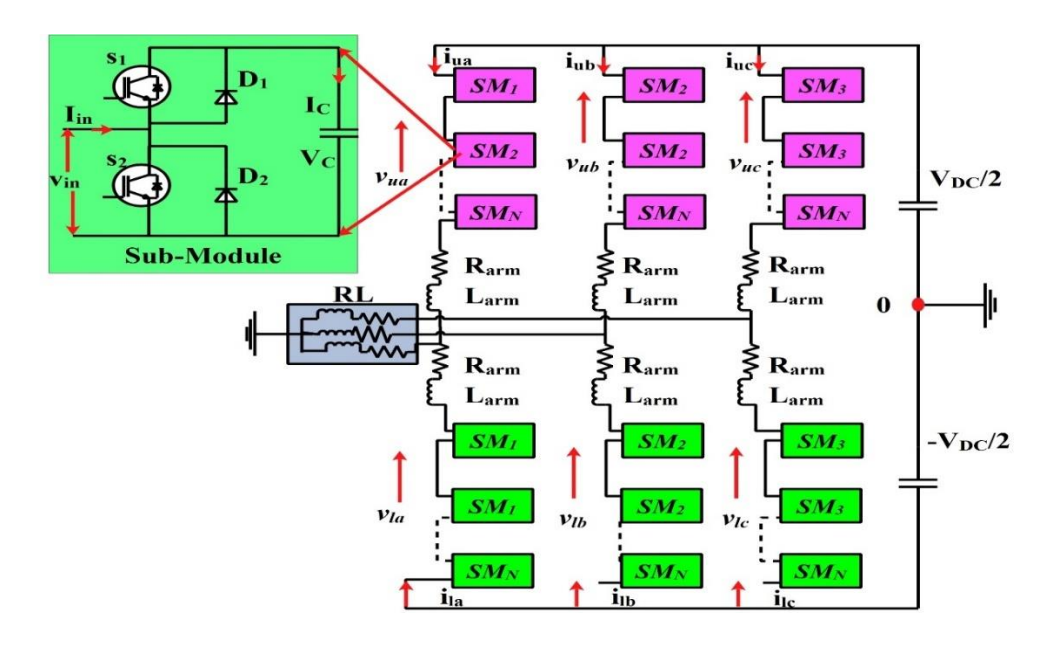


Figure 1 Structure of MMC

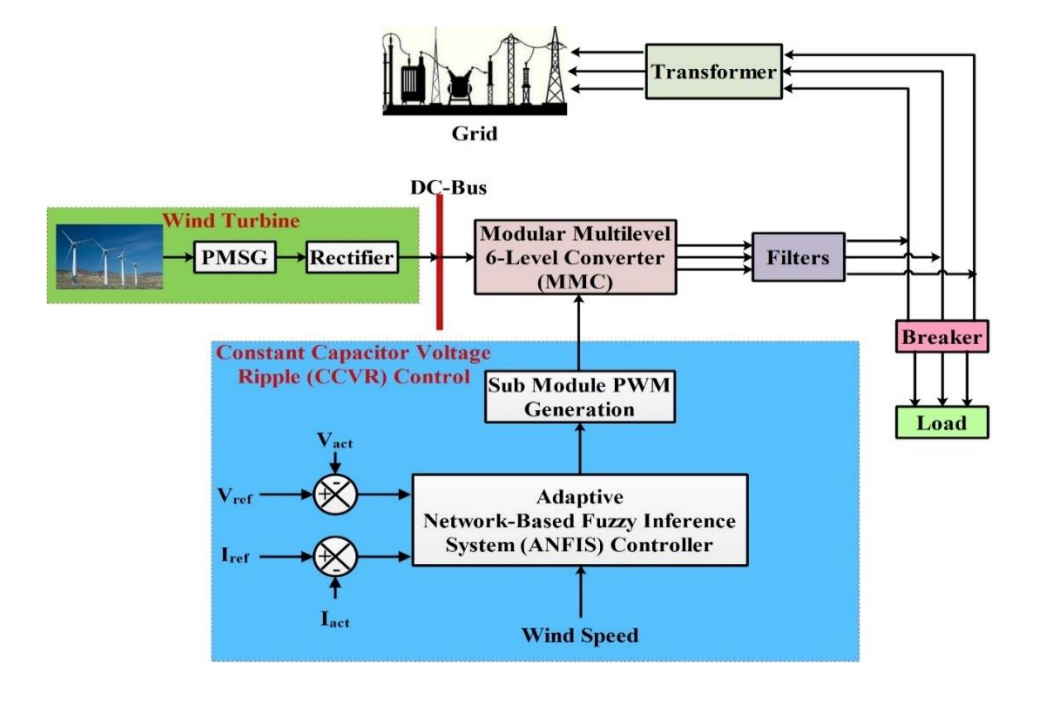


Figure 2 General Block Diagram of the Proposed Method

It shows the proposed system's overall control architecture. The control block diagram of Figure 2 illustrates how the CCVR control of the MMC is split into two sections. In addition to conventional wind control, there is a different kind of circulation injection control. Wind energy conversion systems operate at MPPT sites utilizing traditional wind control to increase conversion efficiency. Circulating current can only be controlled by further injection. The arm current in the MMC will travel via the SM capacitors, unlike two-level converters. Circulating currents will develop due to circular interaction. These currents move around inside the MMC and exit through neither both the AC and DC sides. So, new control parameters can be provided by circulating current. To enhance converter performance. Like controlling output current, circulating current can also be controlled. The ANFIS-based current controller is used to monitor the circulating current's reference value

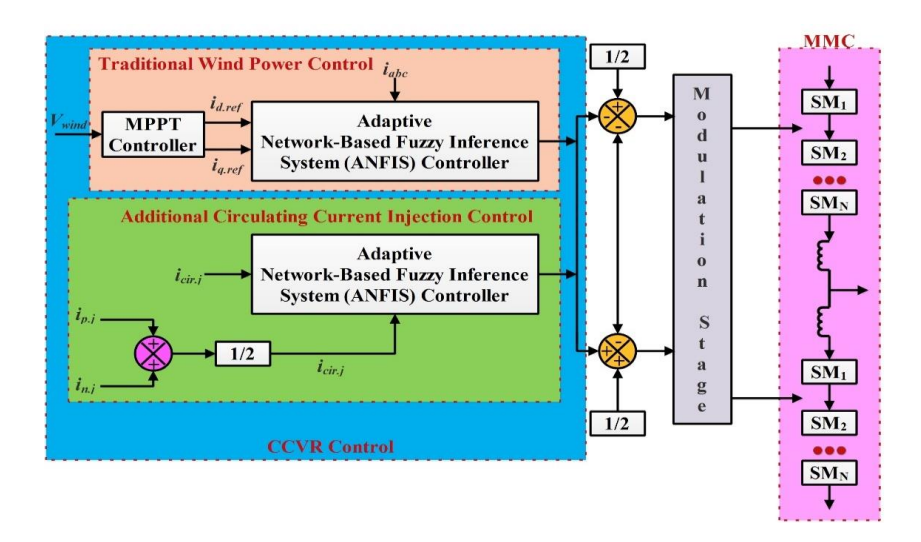


Figure 3 Control Structure of MMC

3.2 Modelling of MMC Based WECS

The mechanical angular velocity and the number of generator poles both have an impact on the MMC's associated PMSG frequency.

$$\omega = \omega_{\rm r} = p \, \omega_{\rm m} \tag{1}$$

The following equations express the MMC's AC-side voltage and current,

$$v_{ac}(t) = V_{AC} Cos(\omega t + \alpha)$$
 (2)

$$i_{ac}(t) = I_{AC} Cos(\omega t + \beta)$$
 (3)

Equation Figure 4 illustrates the connection between the MMC's output current and the PMSG's electromagnetic torque.

$$T_{e}(t) = \frac{3}{2} p \left[\lambda_{m} i_{q}(t) - \left(L_{d} - L_{q} \right) i_{d}(t) i_{q}(t) \right]$$
 (4)

The q-axis and d-axis coupling is broken by controlling the d-axis current to zero. Following that, Eqn. 4 can be shortened in Eqn. 5.

$$\begin{cases} i_d = 0 \\ i_q = \frac{2 T_e}{3 p \lambda_m} \end{cases}$$
 (5)

The details of the wind speed and wind turbine are as follows in Eqn. 5 to include in the electromagnetic torque. In Eqn. 6, their relationship is depicted.

$$T_{e} = \frac{\rho A v_{wind}^{3}}{2 \omega_{m}} C_{p} (\lambda, \beta_{p})$$
 (6)

 C_p should be at its maximum value, shown by $C_{p.max}$, for the wind energy system to achieve MPPT. Consequently, equation (1) can be used to get the reference value of the dq frame 7's output current.

$$\begin{cases} i_{d,ref} = 0 \\ i_{q,ref} = \frac{\rho \pi r_{wind}^3 C_{pmax} v_{wind}^2}{3 p \lambda_m \lambda_{opt}} \end{cases}$$
 (7)

Eqn. 8 states that the three components: DC, phase current, and circulating current make up the arm current of the MMC.

$$\begin{cases} i_{\text{upp}}(t) = \frac{I_{DC}}{3} - \frac{i_{ac}(t)}{2} + i_{\text{cir}}(t) \\ i_{low}(t) = \frac{I_{DC}}{3} + \frac{i_{ac}(t)}{2} + i_{\text{cir}}(t) \end{cases}$$

$$\begin{cases} i_{ac}(t) = I_{AC} \cos(\omega t + \varphi) \\ i_{cir}(t) = I_{C} \cos(2\omega t + \theta_{C}) \end{cases}$$
(8)

The capacitor voltage, for instance, can be calculated, as illustrated below, by integrating the capacitor current using the high-side arm.

$$v_c(t) = V_{c,0} + \frac{1}{C_{SM}} \int i_{ap}(t) S_{upp}(t) dt$$
 (10)

Here,

ω – Angular Speed of MMC

ω_r – Electrical Angular speed of PMSG

p – number of pole pairs

V_{AC} – Output voltage's amplitude

I_{AC} – Output Current's amplitude

 α – Output voltage's phase angle

 β – Output Current's phase angle

 ρ – density of air mass

A - Wind blade area

 $V_{wind} - Wind \ speed$

C_p – Coefficient of performance

 β_p – Pitch angle

 λ – tip-speed ratio

 λ_{opt} – optimum tip-speed ratio

 $r_{wind}-Wind\ blades\ radius$

V_{c,0} - Capacitor voltage's DC Component

C_{SM} – Capacitor value of SM

4. ANFIS Controller Structure

A popular research topic in the present era is the development of a fuzzy logic (FL) and ANN concept for control issues. A reason for this is because a statistical controller design is typically required by the theory of classical control. Particularly for nonlinear as well as intricate challenges to control, controller concert is typically hampered by the imprecision of the plant's mathematical modelling. The introduction of FLCs along with neural controllers based on multi-layered NNs inspired new resources for what may ultimately be a better knowledge of control as well as more efficient control. Fuzzy NN (FNN) is now suggested and progressed in collaboration between FL and NN; typically, this combination is referred to as ANFIS. While a neural network has many inputs and many outputs, a FL network only has many inputs and one output. As a result, an integration of these two is known as an ANFIS, which is recommended for nonlinear applications.

Artificial neural networks and FLC are used to provide Adaptive Neuro-Fuzzy Inference System (ANFIS) controllers. Since they automatically change their parameters in real time for the best control, these controllers are preferred for their performance under a variety of conditions.

The Sugeno Model, which comprises two inputs, one output, and five layers, serves as the basis for the ANFIS architecture. The inputs are initially fuzzed, and subsequently they are defuzzed using an internal rule knowledgebase. Each rule has a weight assigned to it that determines its precedence. The rules and weights can be modified with training to achieve the desired controller response while minimising error. It is possible to write the first order Sugeno model as,

```
u1 is the result if inputs e = A1 \& \Delta e = B1.
u2 is the result if inputs e = A2 \& \Delta e = B2.
Consequently, output u = w1u1 + w2u2
```

A and B are the inputs that have been fuzzified, and w is the selected weight.

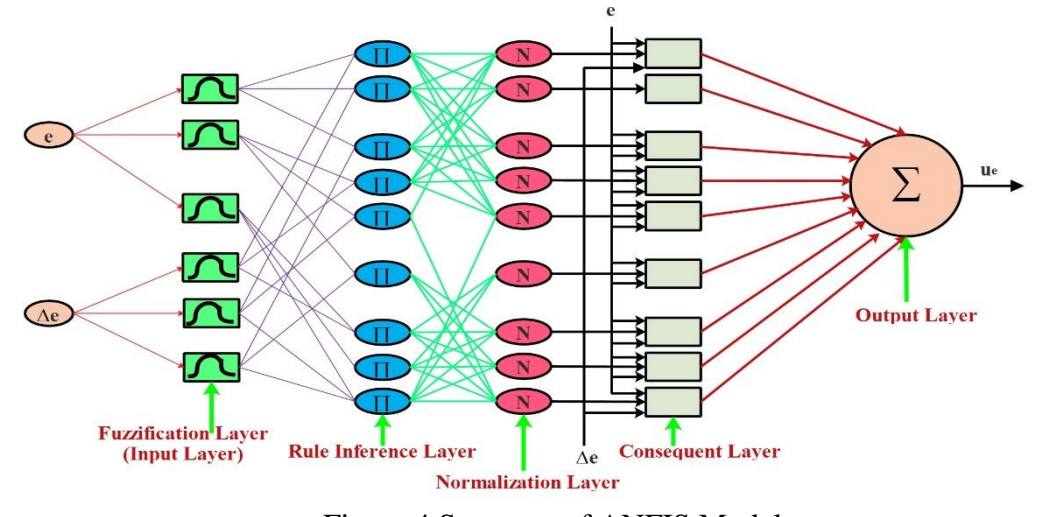


Figure 4 Structure of ANFIS Model

5. Simulation Results and Discussions

The proposed MMC's suggested ANFIS-based controller has been modelled and analysed using a MATLAB/Simulink model, and the results of the examination are reported. Simulation parameters for the MMC-based WECS are listed in Table 1. MATLAB/Simulink simulations demonstrate the effectiveness of the proposed ANFIS-based control strategy.

Table 1: Simulation Parameters

| PMSG | | MMC Values | |
|--------------------------|--------|-----------------------------|--------------|
| Parameter | Value | Parameter | Value |
| Power Rating | 10 kW | Rated Capacity | 5 MVA |
| Frequency of Supply | 50 Hz | DC Link voltage | $\pm~4000~V$ |
| Wind Speed | 12 m/s | SM's count per arm | 4 |
| SM Capacitance | 10 μF | SM Capacitance | 5000 μF |
| • | • | Inductance of each arm | 3 mH |
| Carrier Signal Frequency | 5 kHz | Frequency of Carrier Signal | 2.5 kHz |

Simulation results, depicted in Figures 4-10, illustrate significant reductions in SM capacitor voltage ripple. Notably, the ANFIS controller outperforms the conventional PI controller, achieving a 39% reduction in ripple voltage.

Figures 5-10 represent the waveforms of the WECS. Figure 5 shows the variations of the turbine power for different wind speed and the various wind speeds wrt the time is shown in the figure number 6.

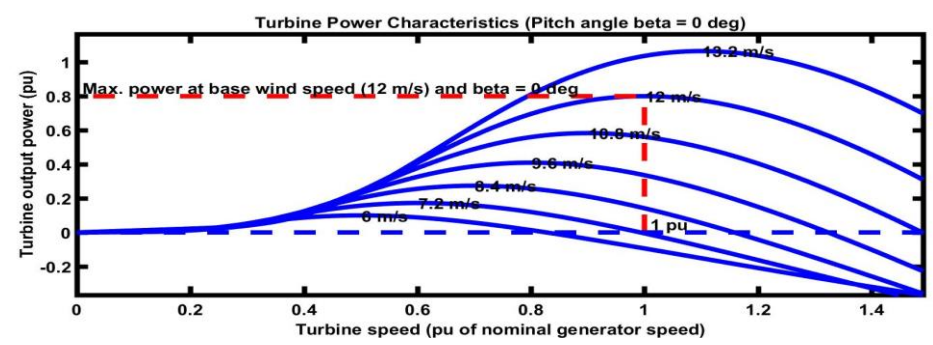


Figure 5Wind Turbine Power Characteristics

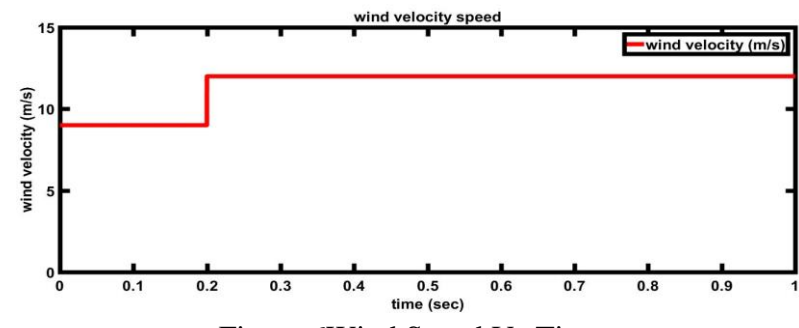


Figure 6Wind Speed Vs Time

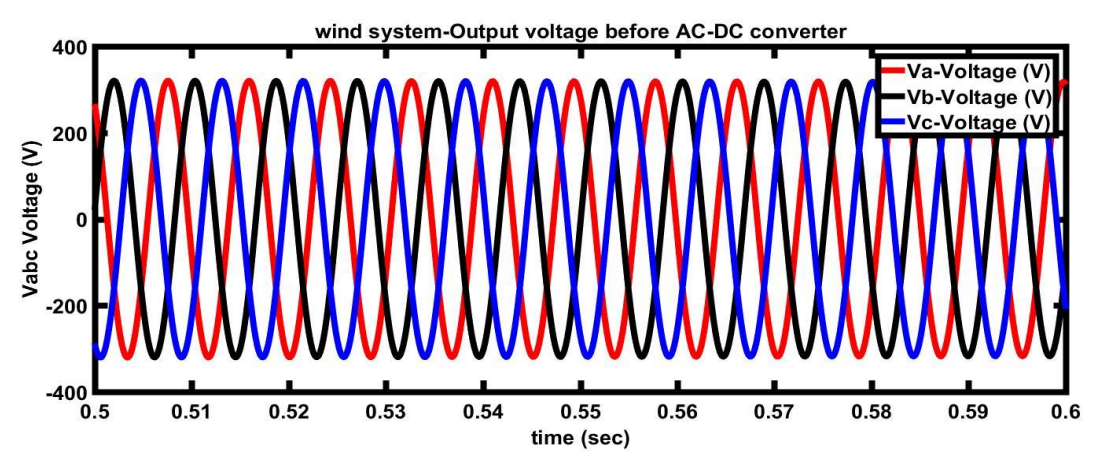


Figure 7 3-phase Output Voltage of PMSG

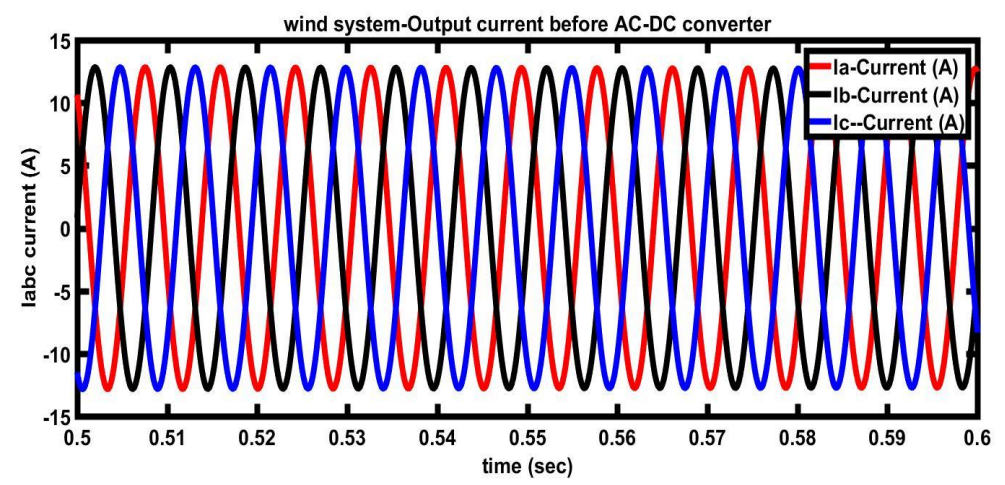


Figure 8 3-phase Output Current of PMSG

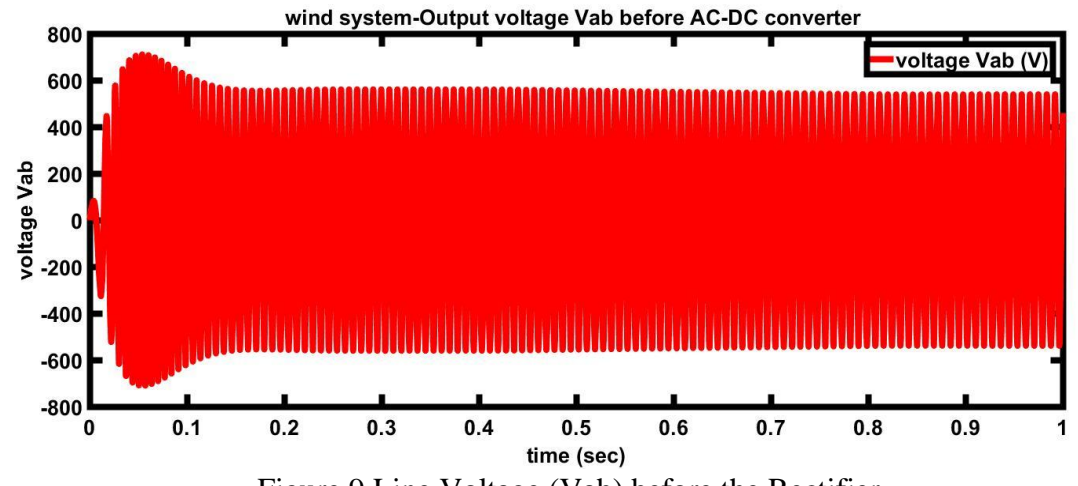


Figure 9 Line Voltage (Vab) before the Rectifier

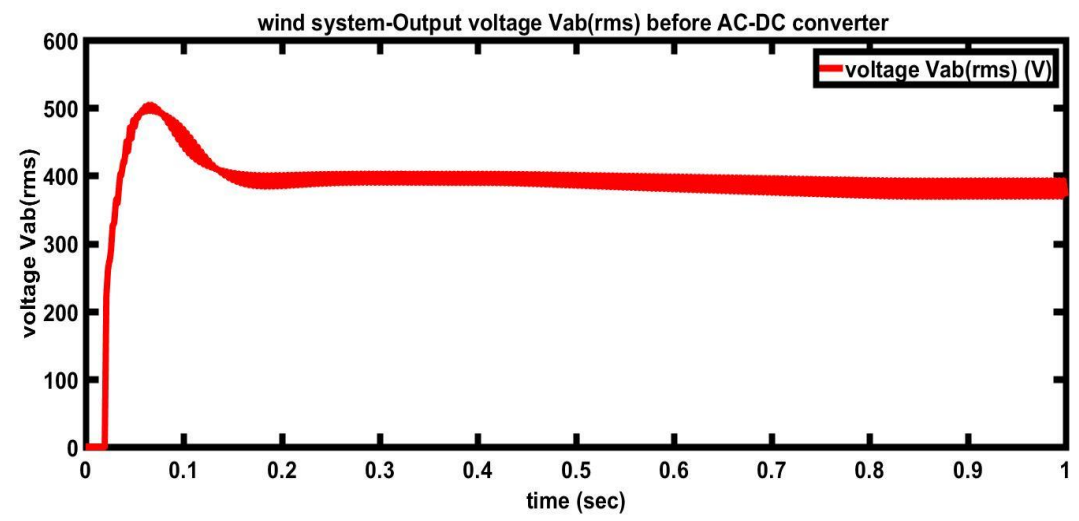


Figure 10 RMS Value of Line Voltage (Vab) before the Rectifier

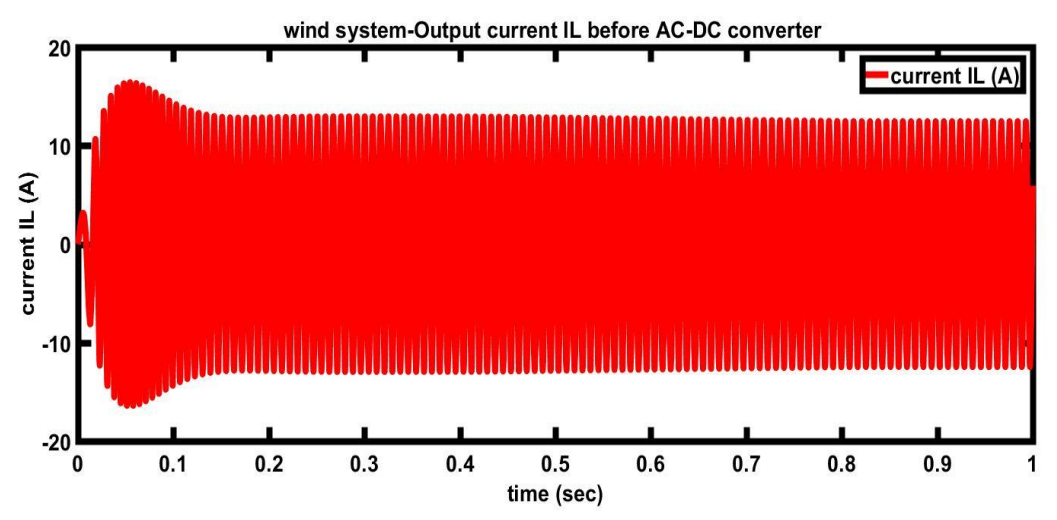


Figure 11 Line Current (I_L) before the Rectifier

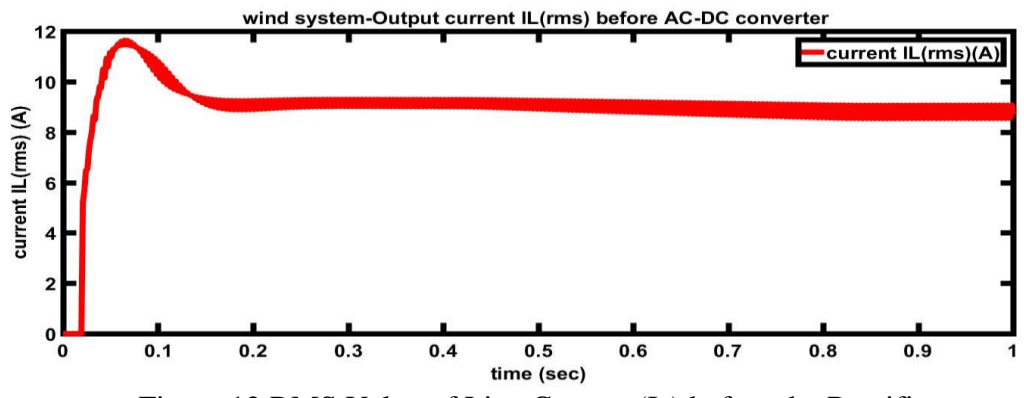


Figure 12 RMS Value of Line Current (IL) before the Rectifier

Figure 13 depicts the change in the rotor speed of the PMSG of the WECS with respect to the time. The mechanical and electrical torque characteristics are portrayed in the Figure 14. The overall power output of the WECS is displayed in the Figure 15.

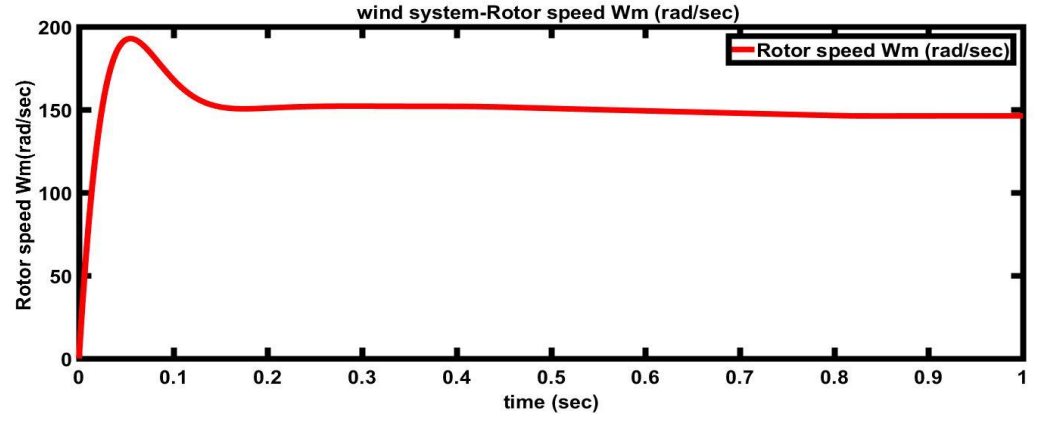


Figure 13 Simulation result of Rotor Speed

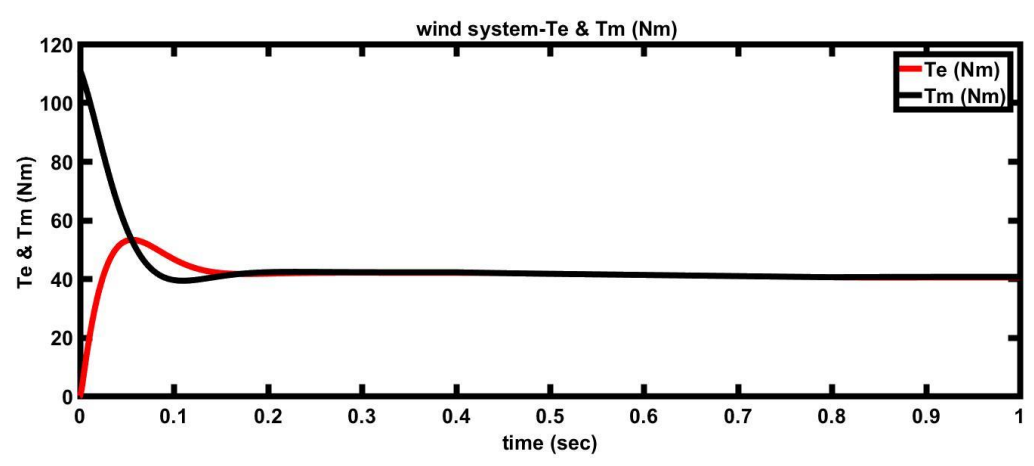


Figure 14 Mechanical & Electrical Torques of Wind Turbine

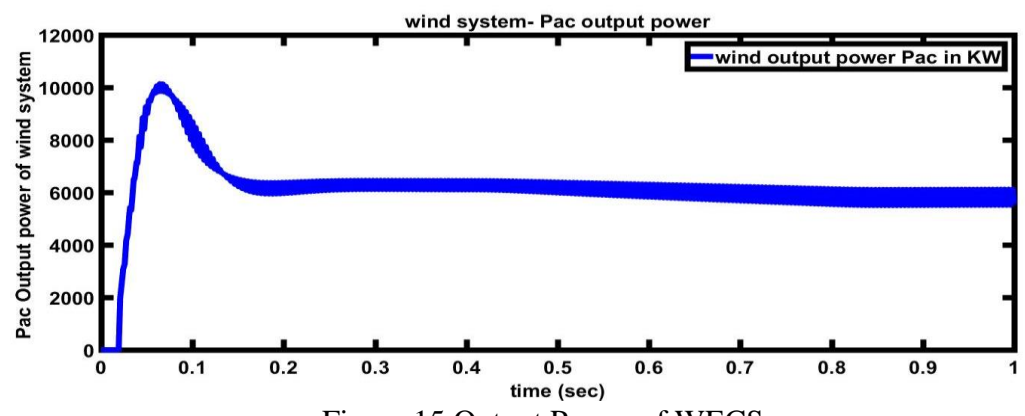


Figure 15 Output Power of WECS

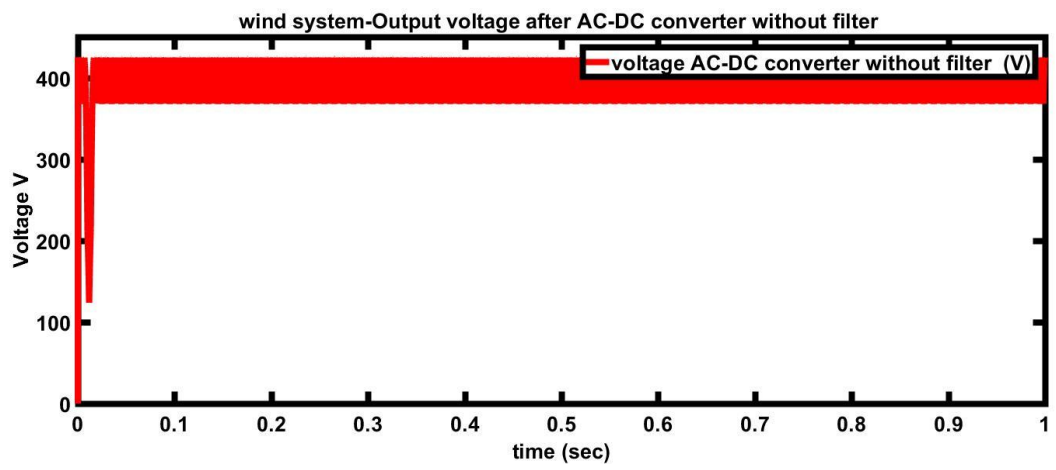


Figure 16 Output Voltage of Rectifier without Filter

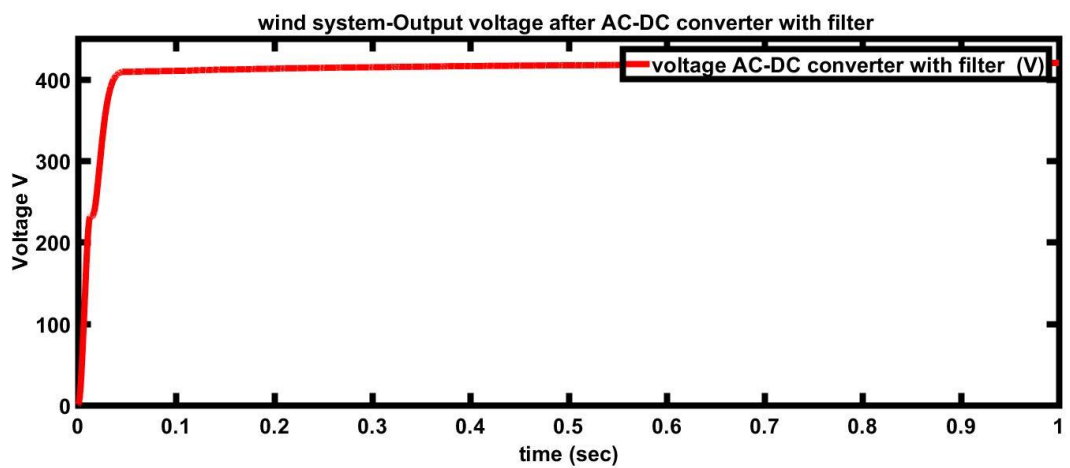


Figure 17 Output Voltage of Rectifier without Filter

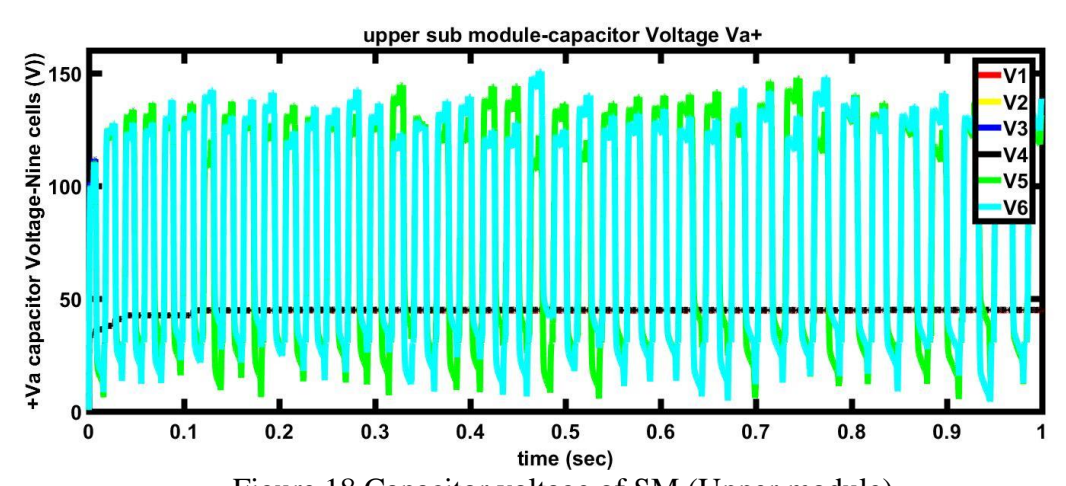


Figure 18 Capacitor voltage of SM (Upper module)

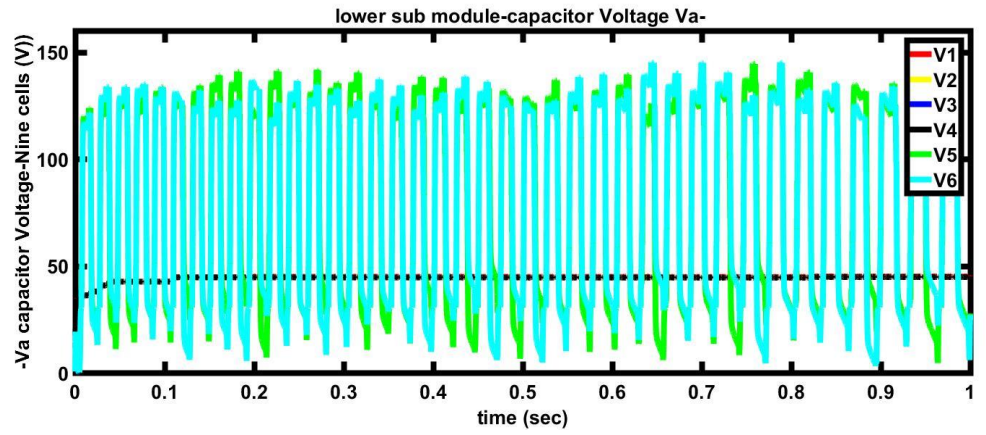


Figure 19 Capacitor voltage of SM (Lower module)

Figure 20-22 illustrates how the three-phase circulating currents and upper and lower arm currents relate to one another.MMC's DC link currents and its actual and reference current values are all displayed in the Figures 23 and 24 respectively. The pulse generated for the MMC and its corresponding reference signal for pulse generation are shown in the figures 25 and 26 respectively.

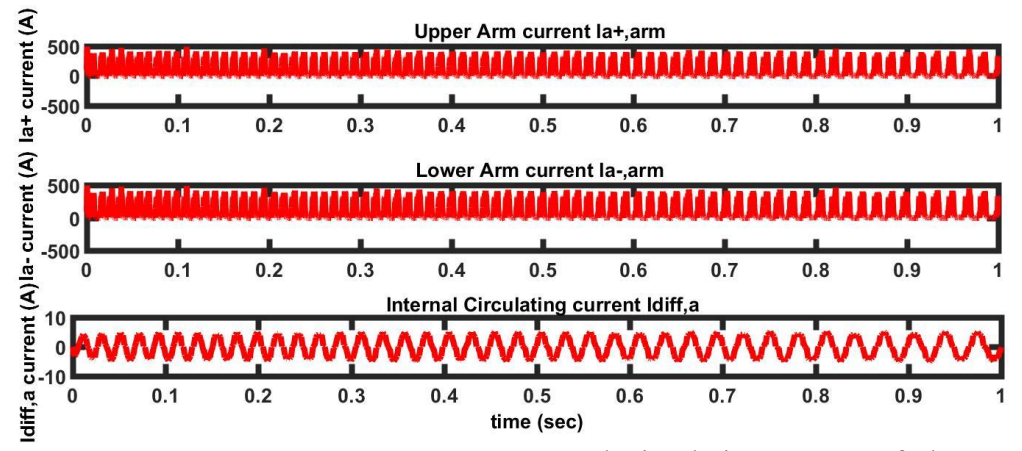


Figure 20 MMC's Arm Currents & Internal Circulating Current of Phase A

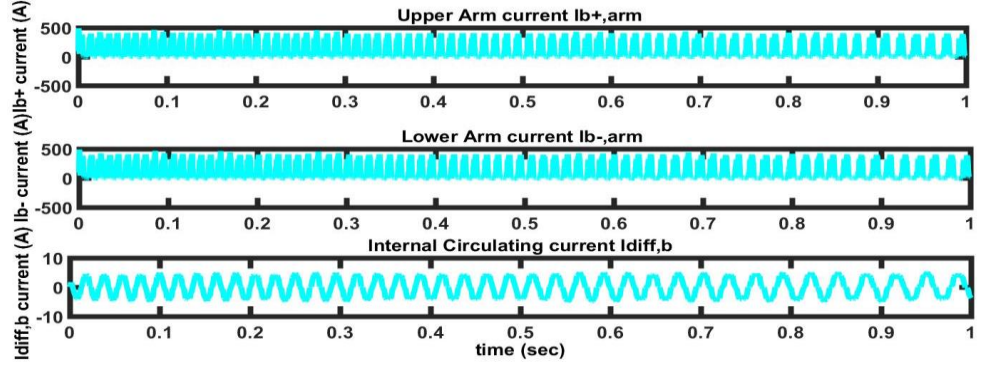


Figure 21 MMC's Arm Currents & Internal Circulating Current of Phase B

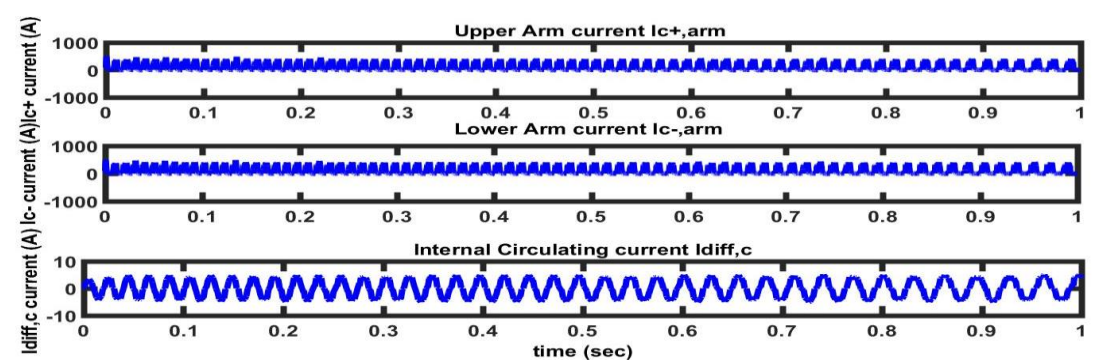


Figure 22 MMC's Arm Currents & Internal Circulating Current of Phase C

DC link current ldc_a, ldc_b, ldc_c

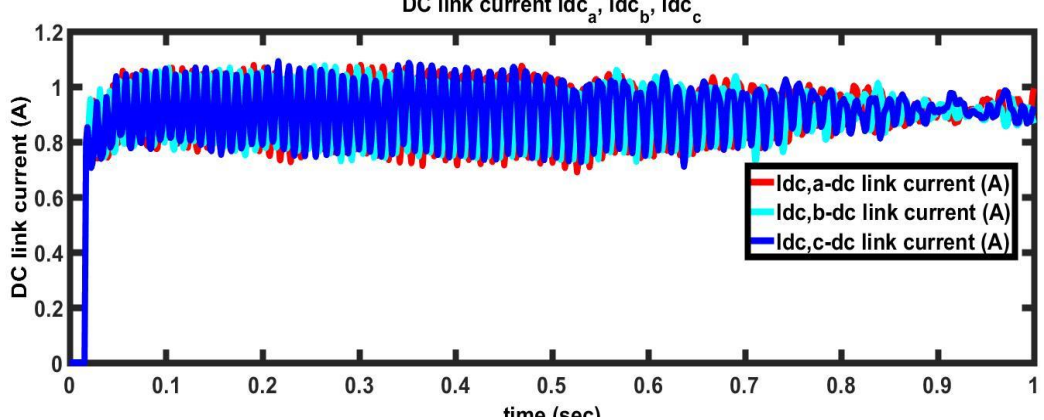


Figure 23 DC-Link Currents all three phases

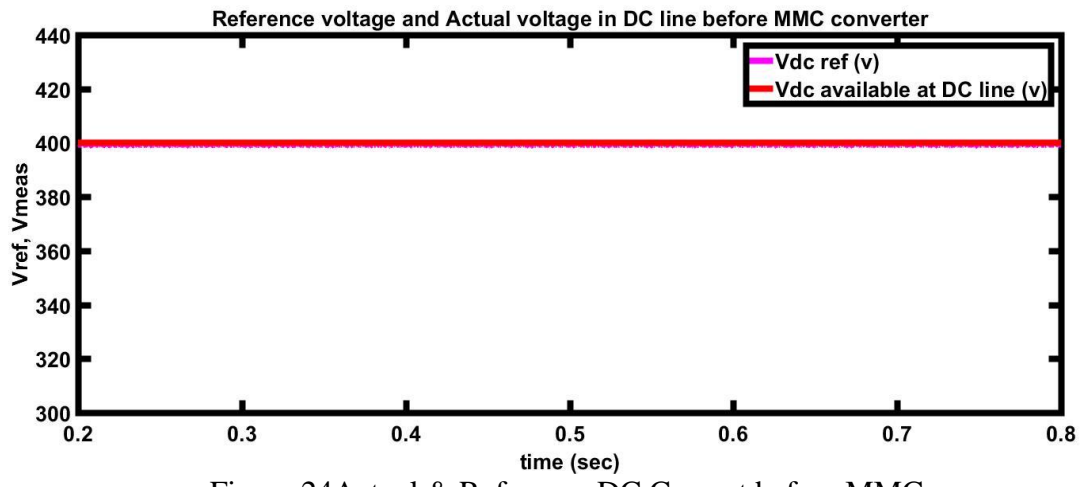


Figure 24Actual & Reference DC Current before MMC

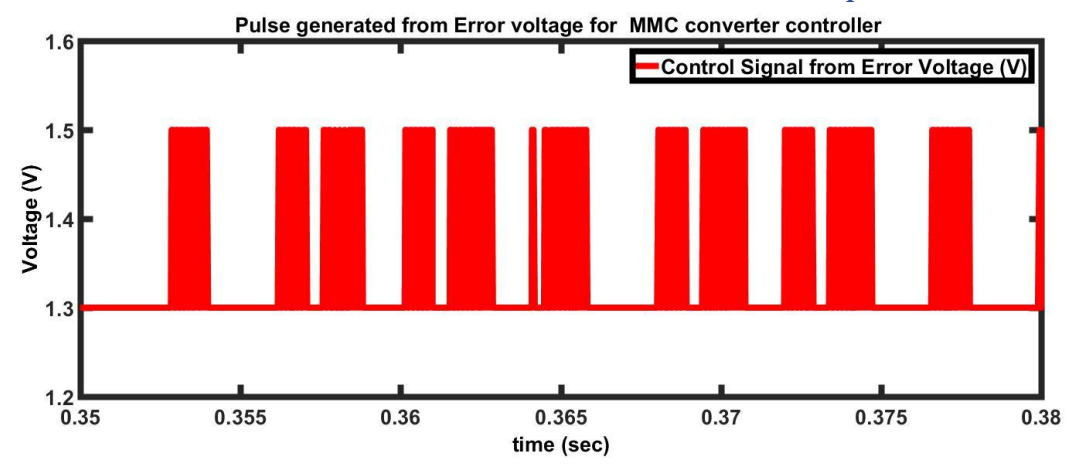


Figure 25 Pulse for MMC

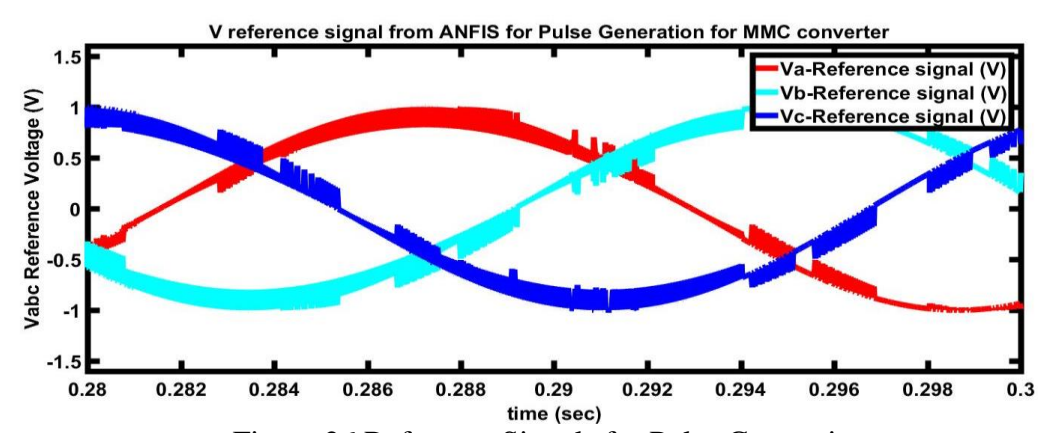


Figure 26 Reference Signals for Pulse Generation

Figure 27 shows the capacitor voltage for the upper sub-module and figure 28 for the lower sub-module. Also, the circulating currents for the PI and the ANFIS controllers are depicted in the figures 29 and 30 respectively.

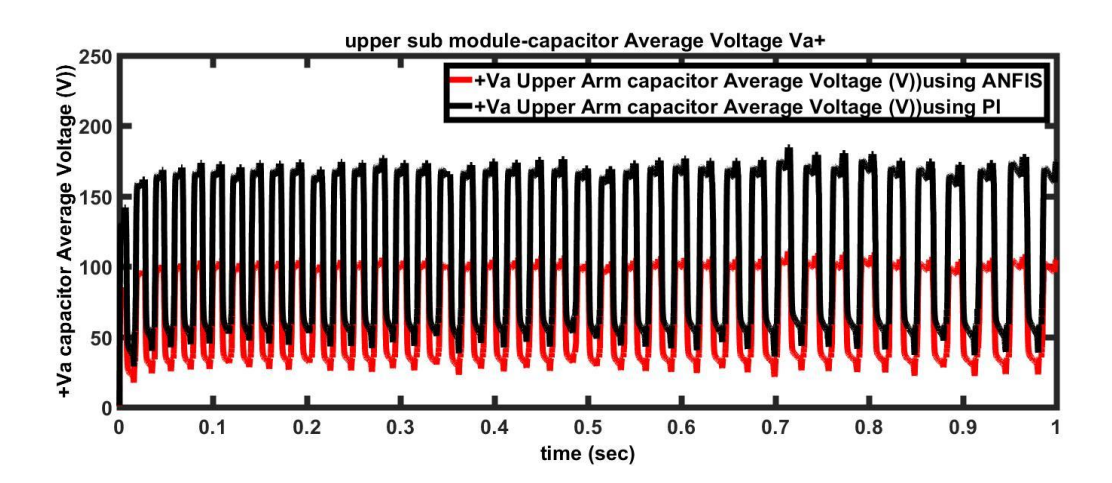


Figure 27 Average Capacitor Voltage of SM (Upper Module) using PI & ANFIS Controllers

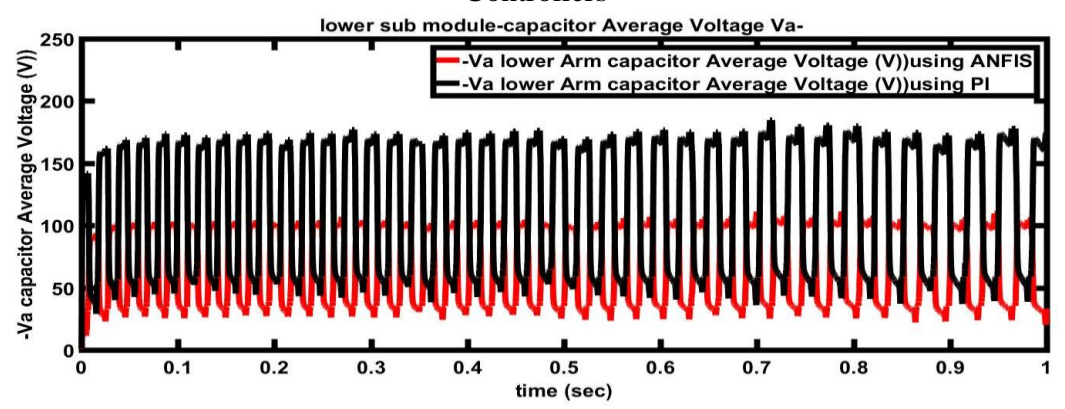


Figure 28Average Capacitor Voltage of SM (Lower Module) using PI & ANFIS Controllers

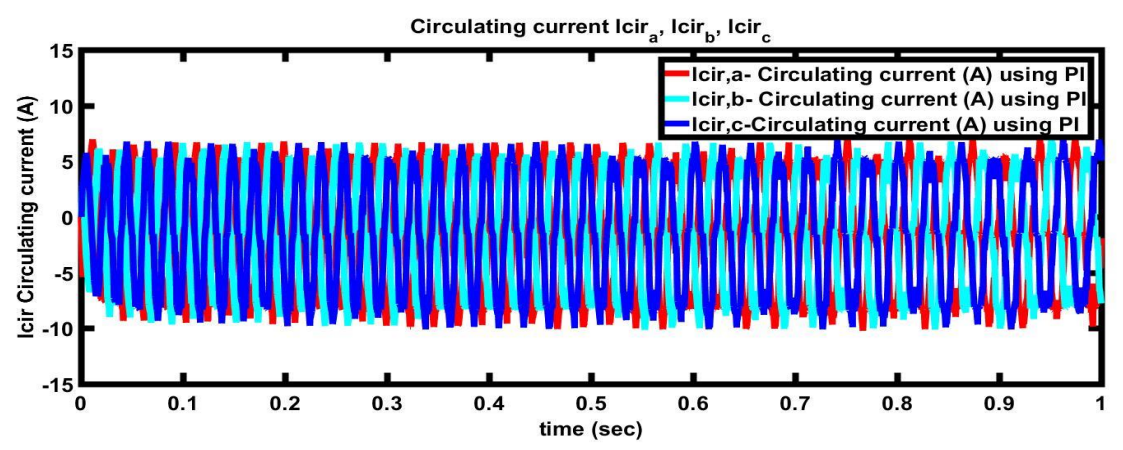


Figure 29 Circulating Current using PI Controller

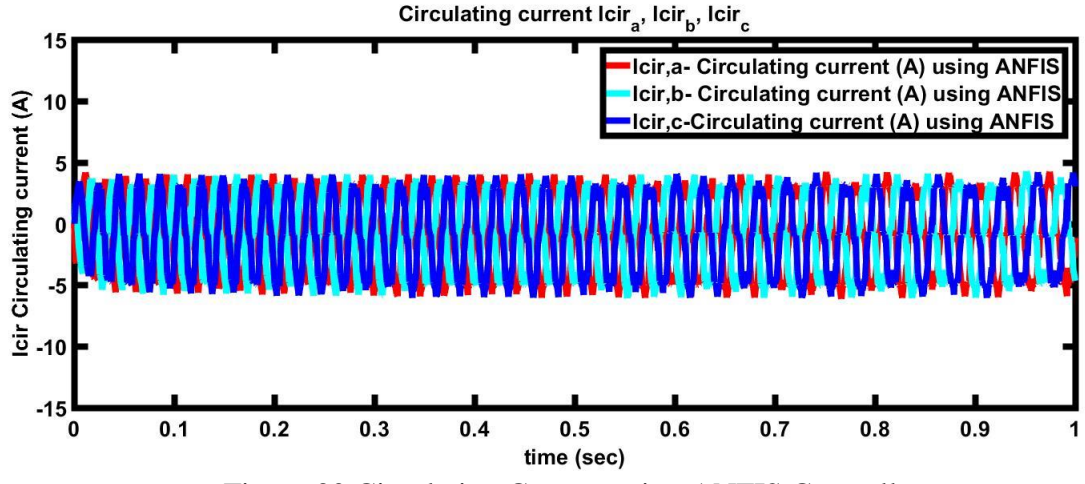


Figure 30 Circulating Current using ANFIS Controller

Again, here we can infer that the circulating currents for the ANFIS controller are smaller for the proposed ANFIS controller. Figure 31 shows the capacitor ripple voltage for the different circulating currents under varying airflow rates. The fluctuations of the capacitor ripple are shown in Figure 32. voltages with wind velocity under different cases namely, with no circulating current injection, with injection of circulating current along with PI controller and lastly with the ANFIS controller. Clearly it can be inferred that the ripple voltage in minimum in the case with ANFIS controller.

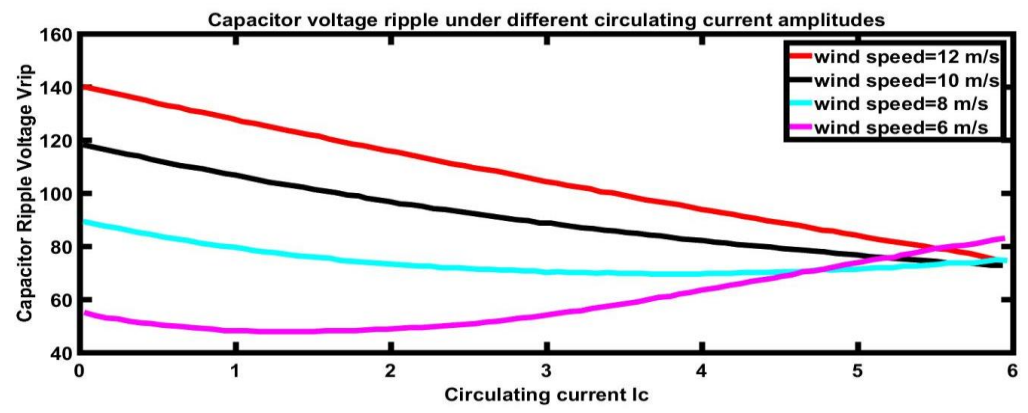


Figure 31 Variations of Capacitor Ripple Voltage for different Circulating Currents generated under various Wind Speeds

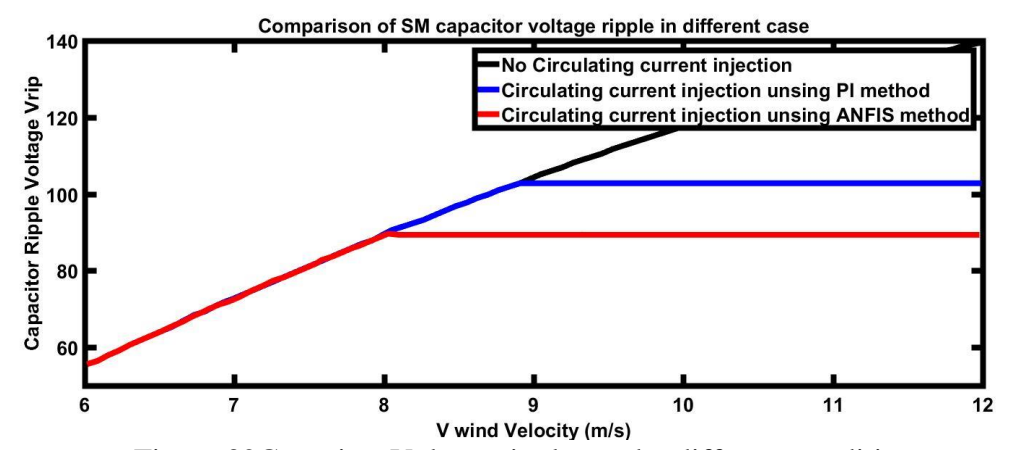


Figure 32Capacitor Voltage ripples under different conditions

6. Conclusion

In the proposed PMSG based WPCS, the varying wind speed causes fluctuations in the PMSG phase current with high amplitude and low frequency which results in SM voltage ripple. This study proposes an ANFIS based control strategy for minimal capacitor voltage ripple regulation. To eliminate ripple on the SM capacitor, the six-level, three-phase WECS of

the proposed control approach, based on MMC, injects the second harmonic component of the circulating current. This control method drastically reduces the voltage ripple where the injected second harmonic component restrains the fundamental component. According to the results, the CM capacitor's voltage fluctuations have been significantly reduced. Results from the PI console and the ANFIS console were contrasted. The ANFIS provides better performance over the PI controller. It is also observed from the results that the average capacitor voltage using ANFIS controller is approximately 100V whereas using the PI controller is 165V at the rated wind velocity of 12m/s. the SM capacitor is also greatly minimized with circulating current injection method compared to PI controller which significantly improve the performance of MMC and reduces the volume and cost of the capacitor.

A new ANN-based MPC controller for a solar power Grid connected system through an alternate arm converter has been proposed designed & verified by simulation studies in this research paper. Since the trained models are constructed with basic arithmetic operations that are unrelated to the complexity of the MPC algorithm, they can effectively minimize the computational cost of real-time control. ANN built ML models are trained to simulate MPC controllers. The suggested AAC is attractive for HVDC systems, according to the theoretical development and given simulation results. When compared to MPC, the suggested ML controller will lower the computational requirements of the controller.

Compliance with Ethical Standards

Disclosure of potential conflicts of interest

The authors declare that they have no competing interests.

Availability of data and materials

Data sharing not applicable to this article as no datasets were generated or analyzed during the current study.

Informed consent

Not Applicable

Funding

This work was supported by the Deanship of Scientific Research, Vice Presidency for Graduate Studies and Scientific Research, King Faisal University, Saudi Arabia [Grant No. KFU242760].

Refrences

[1] Novakovic B, Nasiri A. Modular multilevel converter for wind energy storage applications. IEEE Transactions on Industrial Electronics. 2017 Mar 2;64(11):8867-76.

- [2] Yang S, Fang J, Tang Y, Qiu H, Dong C, Wang P. Modular multilevel converter synthetic inertia-based frequency support for medium-voltage microgrids. IEEE Transactions on Industrial Electronics. 2019 Jan 11;66(11):8992-9002.
- [3] Du S, Wu B, Zargari NR, Cheng Z. A flying-capacitor modular multilevel converter for medium-voltage motor drive. IEEE Transactions on Power Electronics. 2016 May 10;32(3):2081-9.
- [4] Debnath S, Saeedifard M. A new hybrid modular multilevel converter for grid connection of large wind turbines. IEEE Transactions on Sustainable energy. 2013 Sep 16;4(4):1051-64.
- [5] Zhang Y, Ravishankar J, Fletcher J, Li R, Han M. Review of modular multilevel converter based multi-terminal HVDC systems for offshore wind power transmission. Renewable and Sustainable Energy Reviews. 2016 Aug 1; 61:572-86.
- [6] Xiao Q, Mu Y, Jia H, Jin Y, Hou K, Yu X, Teodorescu R, Guerrero JM. Modular multilevel converter based multi-terminal hybrid AC/DC microgrid with improved energy control method. Applied Energy. 2021 Jan 15;282: 116154.
- [7] Zhang Y, Deng F, Hou J, Jiang P, Zhang H, Zhu K, Hu Y, Vazquez S. Cascaded Modular Multilevel Converter and Cycloconverter Based Machine Drive System. IEEE Transactions on Industrial Electronics. 2022 Apr 29.
- [8] de Sousa RO, Cupertino AF, Morais LM, Pereira HA. Wear-out failure analysis of modular multilevel converter-based STATCOM: The role of the modulation strategy and IGBT blocking voltage. Microelectronics Reliability. 2022 Jan 1;128: 114426.
- [9] Huang M. A Non-Isolated DC-DC Modular Multilevel Converter with Proposed Middle Cells. Electronics. 2022 Apr 2;11(7):1135.
- [10] Xiao Q, Mu Y, Jia H, Jin Y, Yu X, Teodorescu R, Guerrero JM. Novel modular multilevel converter-based five-terminal MV/LV hybrid AC/DC microgrids with improved operation capability under unbalanced power distribution. Applied Energy. 2022 Jan 15;306: 118140.
- [11] Liu J, Dong D, Zhang D. A hybrid modular multilevel converter family with higher power density and efficiency. IEEE Transactions on Power Electronics. 2021 Jan 29;36(8):9001-14.
- [12] Reddy AG, Shukla A. The Switched Modular Multilevel Converter: A Compact VSC for High and Medium Voltage Applications. IEEE Transactions on Power Delivery. 2022 Jan 25.
- [13] Rosyadi M, Umemura A, Takahashi R, Tamura J. A Study on Modular Multilevel Converter based Wind Turbine Generator Connected to Medium Voltage DC Collection Network. In2020 2nd International Conference on Broadband Communications, Wireless Sensors and Powering (BCWSP) 2020 Sep 28 (pp. 177-182). IEEE.

- [14] Gontijo G, Wang S, Kerekes T, Teodorescu R. New ac–ac modular multilevel converter solution for medium-voltage machine-drive applications: Modular multilevel series converter. Energies. 2020 Jul 16;13(14):3664.
- [15] Hasan NS, Rosmin N, Osman DA, Musta'amal AH. Reviews on multilevel converter and modulation techniques. Renewable and Sustainable Energy Reviews. 2017 Dec 1;80: 163-74.
- [16] Salem WA, Osman GF, Arfa SH. Adaptive neuro-fuzzy inference system-based field oriented control of PMSM & speed estimation. In2018 Twentieth International Middle East Power Systems Conference (MEPCON) 2018 Dec 18 (pp. 626-631). IEEE.
- [17] Orlowska-Kowalska T, Szabat K. Control of the drive system with stiff and elastic couplings using adaptive neuro-fuzzy approach. IEEE Transactions on Industrial Electronics. 2007 Feb 5;54(1):228-40.
- [18] Altin N, Sefa İ. dSPACE based adaptive neuro-fuzzy controller of grid interactive inverter. Energy Conversion and Management. 2012 Apr 1;56: 130-9.
- [19] El-bakkouri J, Ouadi H, Saad A. Adaptive Neuro Fuzzy Inference System Based controller for Electric Vehicle's hybrid ABS braking. IFAC-PapersOnLine. 2022 Jan 1;55(12):371-6.
- [20] Saju C, Michael PA, Jarin T. Modeling and control of a hybrid electric vehicle to optimize system performance for fuel efficiency. Sustainable Energy Technologies and Assessments. 2022 Aug 1; 52:102087.